

The Plant Journal (2020) 103, 1233-1245

doi: 10.1111/tpj.14798

Multiple ER-to-nucleus stress signaling pathways are activated during *Plantago asiatica mosaic virus* and *Turnip mosaic virus* infection in *Arabidopsis thaliana*

Mathieu Gayral¹, Omar Arias Gaguancela¹, Evelyn Vasquez², Venura Herath^{1,3,4}, Francisco J. Flores^{2,5}, Martin B. Dickman³ and Jeanmarie Verchot^{1,3}*

Received 1 July 2019; revised 2 April 2020; accepted 23 April 2020; published online 11 May 2020. *For correspondence (e-mail Jm.verchot@tamu.edu).

SUMMARY

Pathogens and other adverse environmental conditions can trigger endoplasmic reticulum (ER) stress. ER stress signaling increases the expression of cytoprotective ER-chaperones. The inositol-requiring enzyme (IRE1) is one ER stress sensor that is activated to splice the bZIP60 mRNA that produces a truncated transcription factor that activates gene expression in the nucleus. The IRE1/bZIP60 pathway is associated with restricting potyvirus and potexvirus infection. This study shows that the *Plantago asiatica mosaic virus* (PIAMV) triple gene block 3 (TGB3) and the *Turnip mosaic virus* (TuMV) 6K2 proteins activate alternative transcription pathways involving the bZIP17, bZIP28, BAG7, NAC089 and NAC103 factors in *Arabidopsis thaliana*. Using the corresponding knockout mutant lines, we show that bZIP17, bZIP60, BAG7 and NAC089 are factors in reducing PIAMV infection, whereas bZIP28 and bZIP60 are factors in reducing TuMV infection. We propose a model in which bZIP60 and bZIP17 synergistically induce genes restricting PIAMV infection, while bZIP60 and bZIP28 independently induce genes supporting PIAMV infection. Regarding TuMV-green fluorescent protein (GFP) infection, bZIP60 and bZIP28 serve to repress local and systemic infection. Finally, tauroursodeoxycholic acid treatments were used to demonstrate that the protein folding capacity significantly influences PIAMV accumulation.

Keywords: ER-to-nucleus signaling, unfolded protein response, *Plantago asiatica mosaic virus*, *Turnip mosaic virus*, protein folding capacity.

INTRODUCTION

The endoplasmic reticulum (ER) and Golgi network house the cellular machinery for protein synthesis, maturation and delivery to the intended subcellular compartments. Adverse environmental conditions such as heat, drought and pathogen attack can drastically alter the protein maturation and cause a bottleneck of malformed proteins in the ER (Nawkar et al., 2018; Bao et al., 2019). ER stress sensors recognize the accumulating unfolded proteins, and increase the synthesis of ER-associated chaperones and protein degradation machinery to refold or decay proteins. This unfolded protein response (UPR) serves to alleviate conditions in the ER and

recover homeostasis. When ER stress is chronic and cells cannot be returned to homeostasis, there is heightened autophagy and cell death (Liu *et al.*, 2012; Angelos *et al.*, 2017).

In plants, UPR signaling is mainly mediated by alternative pathways leading to increased expression of genes that restore ER homeostasis (Angelos *et al.*, 2017). One pathway involves the inositol-requiring enzyme (IRE1) and the basic leucine zipper 60 (bZIP60) transcription factor. *Arabidopsis thaliana* has two copies of *IRE1* known as *IRE1a* and *IRE1b* that catalyze splicing of *bZIP60* mRNA (Deng *et al.*, 2013). The bZIP60 transcription factor upregulates the expression of several ER resident chaperones,

¹Texas A&M Agrilife Research and Extension Center in Dallas, 17360 Coit Rd, Dallas, TX, 75252, USA,

²Departamento de Ciencias de la Vida y la Agricultura, Universidad de las Fuerzas Armadas-ESPE, Av. General Rumiñahui s/n y Ambato, Sangolquí 171103, Ecuador,

³Department of Plant Pathology and Microbiology, Institute for Plant Genomics and Biotechnology, Texas A&M University, 498 Olsen Blvd, College Station, TX, 77843, USA,

⁴Department of Agricultural Biology, Faculty of Agriculture, University of Peradeniya, Peradeniya 20400, Sri Lanka, and ⁵Centro de Investigación de Alimentos, CIAL, Facultad de Ciencias de la Ingeniería e Industrias, Universidad Tecnológica Equinoccial-UTE, Av. Mariscal Sucre y Mariana de Jesús, Quito, Pichincha, 170129, Ecuador

including protein disulfide isomerase (PDI), calnexin (CNX), calreticulin (CRT) and the HSP70-like binding immunoglobulin protein (BiP; Iwata and Koizumi, 2005). A separate branch of the IRE1-led pathway targets mRNAs of secreted proteins in a process called regulated IRE1-dependent decay of mRNAs (RIDD). The RIDD activity of IRE1b is linked to the activation of autophagy in response to ER stress (Bao and Howell, 2017; Bao et al., 2018; Srivastava et al., 2018).

The second major pathway is mediated by bZIP17 and bZIP28. These transcription factors have transmembrane domains and normally reside in the ER (Che et al., 2010; Angelos et al., 2017). The AtbZIP17 is activated following salt stress, while AtbZIP28 is activated by heat or chemical stress. The bZIP28 resides in the ER as part of a complex with the Bcl-2-associated athanogene 7 (BAG7) and BiP (Srivastava et al., 2013; Li et al., 2017). Upon activation, the BAG7/bZIP28/BiP complex dissociates. The bZIP17 and bZIP28 migrate from the ER to the Golgi where the SITE-1 protease (S1P) and S2P remove the transmembrane domains (Iwata and Koizumi, 2005; Iwata et al., 2009, 2017; Sun et al., 2013a). These bZIP factors enter the nucleus where they activate expression of BiPs and other chaperones, similar to bZIP60. The bZIP17, bZIP28 and bZIP60 form homo- and heterodimers in the nucleus (Deppmann, 2004; Vinson et al., 2006; Nawkar et al., 2018). The transmembrane domain of BAG7 is also proteolytically removed, and the truncated BAG7 translocates to the nucleus independent of bZIP28. BAG7 interacts with WRKY29 and induces transcription of stress-responsive chaperones, including BAG7 itself. BAG7/WRKY29 transcribe cytoprotective genes (Li et al., 2017).

The bZIP60, bZIP28 and bZIP17 factors commonly recognize G-box core promoter sequences (CACGTG). The sequences flanking the G-box provide specificity for attracting homo-and heterodimeric bZIP factors. However, we do not know enough to predict dimeric pairs controlling transcription patterns (Ezer et al., 2014, 2017). Nevertheless, experiments have demonstrated that the bZIP60 and bZIP28 recognize the promoters of at least two NAC (NAM/ATAF/CUC) transcription factors (Sun et al., 2013b; Nawkar et al., 2018). NAC103 is activated by bZIP60 through the UPRE-III cis-elements and upregulates the expression of genes that are categorically described as 'pro-survival' factors. NAC089 is regulated by bZIP28 and bZIP60 heterodimers through the UPRE and ERSE-I cis-elements, and the protein has a transmembrane domain and localizes to the ER (Yang et al., 2014). In Nicotiana benthamiana, silencing of NbbZIP28 or NbNAC089 increases plant susceptibility to Tobacco mosaic virus (TMV) and Cucumber mosaic virus (CMV; Park et al., 2017; Shen et al., 2017; Li et al., 2018). During ER stress, NAC089 promotes transcriptional activation of BCL2-associated athanogene 6 (BAG6). BAG6 is a co-chaperone with a calmodulin-binding

domain, and has the ability to activate autophagy required for basal immunity against the necrotrophic fungus *Botrytis cinerea* (Yang *et al.*, 2014; Li and Dickman, 2016; Li *et al.*, 2016).

During Plantago asiatica mosaic virus (PIAMV; genus Potexvirus) and Turnip mosaic virus (TuMV; genus Potyvirus) infection, organellar membranes, including the ER, are rearranged creating microenvironments that support replication and guide cell-to-cell movement (Verchot-Lubicz et al., 2010; Grangeon et al., 2013; Tilsner et al., 2013; Verchot, 2016; Cabanillas et al., 2018). These microenvironments concentrate viral proteins necessary for replication and provide protection against cell defenses. The potyvirus membrane-binding protein 6K2 and potexvirus triple gene block 3 (TGB3) are essential for virus replication and movement. Each viral protein of TuMV and Potato virus Y (PVY; genus Potyvirus) as well as PIAMV and Potato virus X (PVX; genus Potexvirus) protein was transiently expressed in N. benthamiana or Arabidopsis leaves, and it was demonstrated that the potyvirus 6K2 and potexvirus TGB3 proteins induce the IRE1/bZIP60 pathway (Yang and Zhang, 2015; Gaguancela et al., 2016). Green fluorescent protein (GFP) was introduced into the infectious clones of PIAMV and TuMV to visualize and quantify virus accumulation in plants. We used GFP to demonstrate that PIAMV-GFP and TuMV-GFP accumulate to higher levels in local and systemic leaves in ire1a/ire1b and bzip60 mutants than wild-type (WT) Col-0 plants. Moreover, we reported that TGB3 preferentially engages IRE1a, whereas 6K2 preferentially engages IRE1b in Arabidopsis plants.

This study shows that bZIP17 and bZIP28 are engaged in UPR responses to infection by PIAMV-GFP and TuMV-GFP in Arabidopsis plants. Our results reveal that multiple ER-to-nucleus stress signaling pathways respond to TGB3 and 6K2 proteins. These alternative UPR pathways converge to mainly restrict PIAMV-GFP and TuMV-GFP accumulation in plants through enhancing the protein folding capacity of the ER.

RESULTS

The potexvirus TGB3 and potyvirus 6K2 induce expression of bZIP60, bZIP28 and bZIP17

The potexvirus TGB3 and potyvirus 6K2 were reported to trigger higher transcript levels of bZIP60 and other chaperones in N. benthamiana or WT Col-0 leaves (Zhang $et\ al.$, 2015; Gaguancela $et\ al.$, 2016). Here, we delivered the PIAMV TGB3, PVX TGB3, PVY 6K2 or TuMV 6K2 genes to Col-0 leaves (n=3 plants), and used reverse transcriptase-quantitative polymerase chain reaction (RT-qPCR) to measure bZIP17, bZIP28, as well as bZIP60 transcript levels. The mock controls were treated with $Agrobacterium\ tume-faciens$ cultures containing empty vectors. Infiltrated leaves

were pooled for RNA extraction at 2 and 5 days post-inoculation (dpi). The RT-qPCRs were performed with the three experimental replicates to obtain the average RNA levels relative to the mock-treated control. Experiments were repeated multiple times to check reproducibility.

At 2 dpi, bZIP17, bZIP28 and bZIP60 transcripts were elevated between two- and 11-fold above the control, following expression of each TGB3 or 6K2 gene (Figure 1a; P < 0.05). At 5 dpi, bZIP60 remained elevated in all samples (P < 0.05). The bZIP17 transcripts declined to control levels, except in PVX TGB3-treated leaves. The bZIP28 transcripts also declined but remained above the control in PIAMV TGB3- and PVY 6K2-expressing leaves (Figure 1b; P < 0.05).

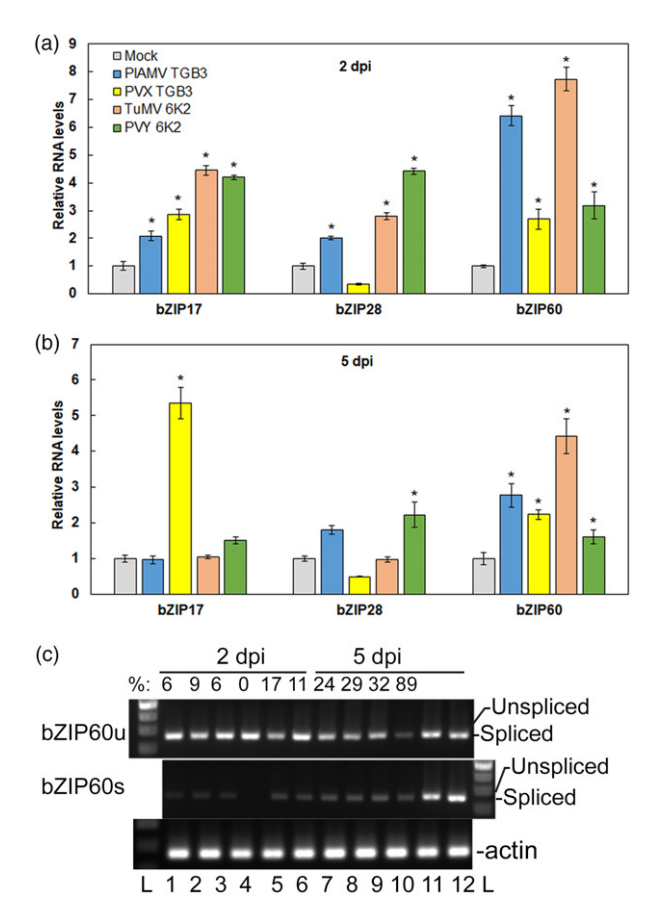


Figure 1. TGB3 and 6K2 induce transcription of bZIP17 bZIP28 and bZIP60 genes in Arabidopsis Col-0 leaves.

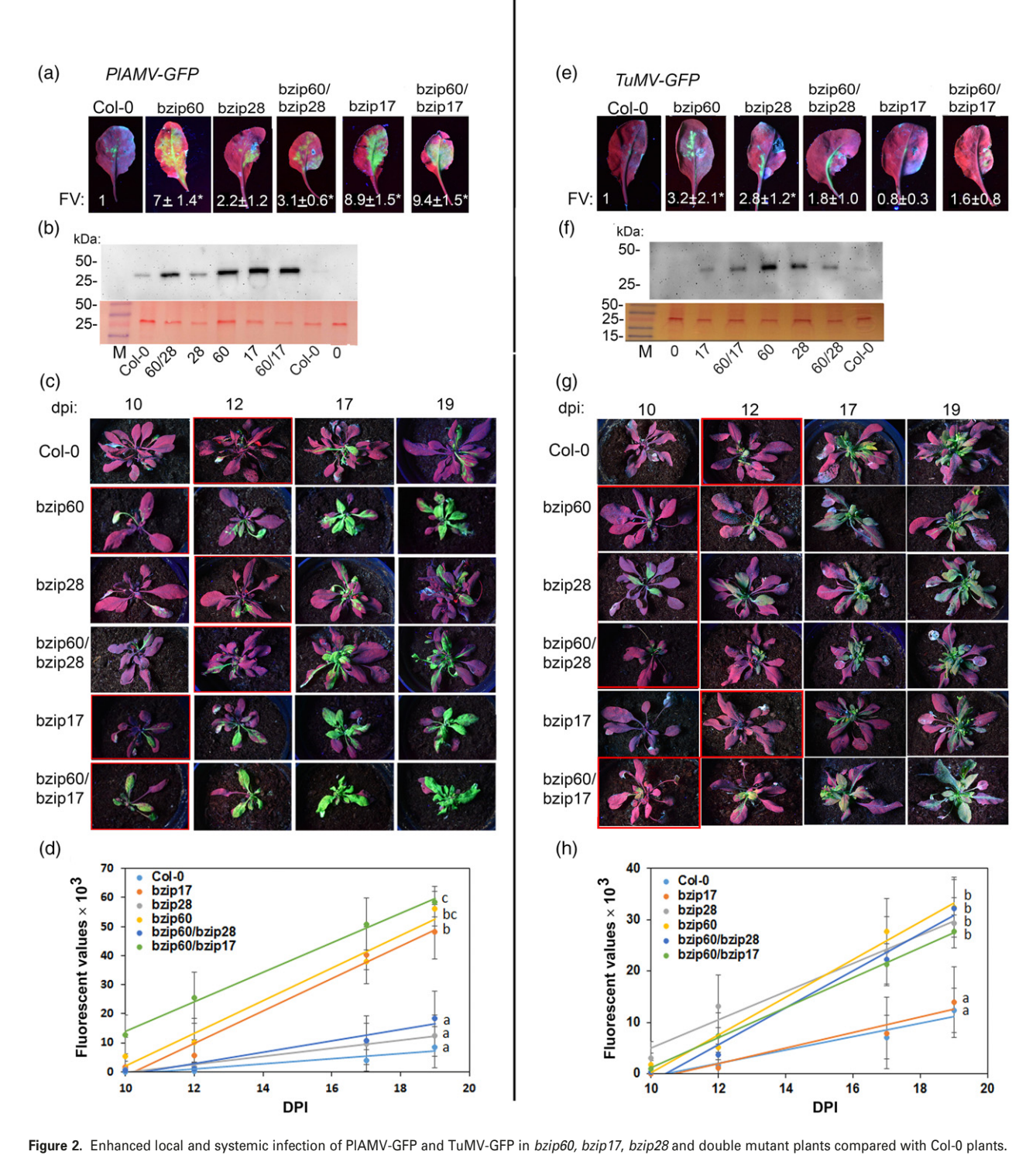
(a,b) Reverse transcriptase-quantitative polymerase chain reaction (RTqPCR) results providing relative RNA levels of bZIP17, bZIP28, bZIP60 following treatments with each viral factor at 2 and 5 days post-inoculation (dpi). Error bars represent the standard deviation (SD); asterisks indicate significant differences to the mock control: Student's *t*-test; P < 0.05; n = 3. (c) Endpoint RT-PCR show accumulation of bZIP60u (top gel) and bZIP60s (bottom gel) transcripts at 2 and 5 dpi. The unspliced PCR product is 139 bp and the spliced PCR product is 116 bp. L, represents lanes with 100 bp ladder. Lanes 1, 6 are Mock; lanes 2, 7 are TuMV 6K2; lanes 3, 8 are PIAMV TGB3; lanes 4, 9 are PVX TGB3; lanes 5, 10 are PVY 6K2; lanes 11, 12 are control products for unspliced and spliced mRNAs on both gels.

The AtbZIP60 mRNA is unconventionally spliced in the cytoplasm by IRE1. We employed the bZIP60 UR primer that spans each side of the 23-nt intron, and a forward bZIP60 primer that would only amplify the spliced Atb-ZIP60 transcripts (AtbZIP60s). We also employed a reverse primer that contains sequences within the spliced region along with the same forward primer to amplify the fulllength AtbZIP60 transcripts (AtbZIP60u). Agro-infiltration was used to deliver the TuMV 6K2, PIAMV TGB3, PVX TGB3 and PVY 6K2 to WT Col-0 leaves. Mock controls were agro-infiltrated to deliver an empty plasmid vector. RNA was extracted at 2 and 5 dpi, and endpoint PCR was used to detect the accumulation of the bZIP60u (270-bp PCR product) and bZIP60s (262-bp PCR product) transcripts. We used densitometry to measure the relative levels of bZIP60s to bZIP60u as a percentage of the combined band intensities. The bZIP60 mRNA is spliced in the mock-treated samples accumulating the bZIP60s to 6% at 2 dpi and 11 % at 5 dpi (Figure 1c). The relative levels of bZIP60s transcripts in leaves expressing the 6K2 or TGB3 genes were between 0 and 9% at 2 dpi, but were between 24 and 89% at 5 dpi. These data show that these viral proteins elicit bZIP60 mRNA splicing. Similar results were reported previously in Gaguancela et al. (2016) using similar primers to demonstrate that these viral elicitors induce bZIP60 mRNA splicing in a manner that is dependent upon IRE1a and IRE1b (Nagashima et al., 2011).

bZIP60 and bZIP17 significantly reduce PIAMV-GFP accumulation

Homozygous bzip60, bzip28 and bzip17 knockout (KO) and WT Col-0 plants were inoculated with PIAMV-GFP. We also agro-inoculated the double KO bzip60/bzip17, bzip60/bzip28 plants. Plants were monitored for green fluorescence each day using a hand-held UV lamp (Figure S1a), and PIAMV-GFP fluorescence was first seen in the inoculated WT and mutant leaves at 4 dpi. We identified 5 dpi to measure the average GFP fluorescence values (FVs) in all plants (Figure S1a). The average FVs were significantly higher in the bzip60, bzip17, bzip60/17 and bzip28/bzip60 leaves (between 3.1- and 9.4-fold; P < 0.05, n = 6) than in WT Col-0 leaves (Figure 2a). The average FVs in bzip28 and WT Col-0 leaves were not different. Immunoblots revealed higher levels of CP at 5 dpi in bzip60, bzip17, bzip60/bzip17 and bzip60/ bzip28 KO than in bzip28 KO or WT Col-0 leaves (Figure 2b). These data suggest that bZIP60 and bZIP17 play greater roles than bZIP28 in restricting PIAMV-GFP local infection.

To learn if these bZIP factors contribute to systemic virus infection, we monitored GFP spread into the upper leaves over 19 days. Although GFP continued to spread beyond 19 dpi, the average FVs showed a linear increase between 10 and 19 dpi. This allowed us to compare FVs between infected mutant KO and WT Col-0 plants (Figure S1a). In these and subsequent experiments, fluorescent images



(a,e) Representative images of PIAMV-GFP and TuMV-GFP inoculated leaves at 5 and 8 days post-inoculation (dpi), respectively. The average fluorescence value (FV) and SD is reported below each image, and the asterisks indicate statistical differences: Student's *t*-test; *P* < 0.05; *n* = 6.

(b,f) Immunoblots detecting PIAMV and TuMV CPs in the inoculated leaves at 5 dpi. Ponceau S-stained membranes below the blots show equal protein loading. Each *bzip* mutant host is identified below each lane. M = molecular weight marker; "0" is mock.

(c,g) Representative images of plants infected with PIAMV-GFP and TuMV-GFP at 10, 12, 17 and 19 dpi. Red boxes surround the plants at 10 or 12 dpi showing the first systemic fluorescence, which in some cases was a small area of a single leaf and in other cases was a broad area.

(d,h) Scatter plots show the average FVs, SDs and trend lines for mutant and Col-0 plants inoculated with PIAMV-GFP and TuMV-GFP. Letters on the right of

each line represent the statistical relatedness of the FVs for each treatment and at each time point as determined by ANOVA; P < 0.05; n = 6.

were captured at 10, 12, 15, 17 and 19 dpi (Figure 2c). We noted that GFP was first seen at 10 dpi in the upper leaves of bzip60, bzip17 and bzip60/zip17 plants, but was seen at 12 dpi in Col-0, bzip28 and bzip60/28 plants (Figure 2d). Systemic FVs were quantified using Image J, and the average FVs were plotted and statistically analyzed (Figure 2d; P < 0.05, n = 6). The average FVs due to PIAMV-GFP in systemic tissues increased at a high rate in bzip60, bzip17 and bzip60/bzip17 plants, and were statistically different from the average FVs calculated in Col-0 plants (Figure 2d; P < 0.05, n = 6). PIAMV-GFP accumulation is significantly higher in bzip60/bzip17 than in bzip17 plants. However, there is no significant difference between bzip60 and bzip60/bzip17 plants, suggesting that bZIP60 and bZIP17 do not have additive effects. The average FVs in Col-0, bzip28 and bipz60/bzip28 plants were not significantly different from each other (Figure 2d; P < 0.05). These combined results indicate that bZIP60 and bZIP17 contribute to restricting the local and systemic infection of PIAMV-GFP, whereas bZIP28 does not restrict PIAMV-GFP infection.

bZIP60 and bZIP28 significantly reduce TuMV-GFP accumulation

Homozygous bzip60, bzip28 and bzip17, bzip60/bzip17, bzip60/bzip28 and WT Col-0 plants were inoculated with TuMV-GFP. Using a hand-held UV lamp, we noted that TuMV-GFP infection is slower to progress than PIAMV-GFP (Figure S1a). TuMV-GFP fluorescence first appeared in the WT Col-0 inoculated leaves at 6 dpi. We identified 8 dpi to measure the average GFP FVs in WT and mutant plants. The average FVs in the TuMV-GFP inoculated leaves of bzip60 and bzip28 plants were significantly higher than in Col-0 plants (Figure 2e; P < 0.05, n = 6), whereas the average FVs in bzip17 leaves were not different from the average FVs in Col-0 leaves. Virus CP accumulation was higher in bzip60, bzip28, bzip60/bzip17 and bzip60/bzip28 infected leaves than in Col-0 infected leaves (Figure 2e). These data suggest that bZIP60 and bZIP28, but not bZIP17, contribute to the ability of TuMV-GFP to establish local infection.

To learn if these bZIP factors contribute to TuMV-GFP systemic infection, we studied GFP fluorescence in systemic tissues over a period of 19 days, and determined the best times to capture images (Figure S1a). Similar to the experiments involving PlaMV-GFP, we recorded fluorescent images at 10, 12, 15, 17 and 19 dpi (Figure 2g). Systemic GFP fluorescence first appeared in the upper leaves of bzip60, bzip28, bzip60/bzip28 and bzip60/bzip17 plants at 10 dpi, and in WT Col-0 and bzip17 plants at 12 dpi. The average GFP FVs were quantified using Image J software and statistically analyzed. The average GFP FVs were significantly higher in bzip60, bzip28, bzip60/bzip28 and bzip60/bzip17 plants than in bzip17 or Col-0 plants (Figure 2g; P < 0.05, n = 6). These results reveal that bZIP60 and bZIP28 restrict TuMV-GFP local and systemic infection.

However, the average FVs were not significantly different among bzip60, bzip28 and bzip60/bzip28 plants, suggesting that bZIP60 and bZIP28 do not have an additive effect.

BAG7 reduces the local accumulation of PIAMV-GFP but not TuMV-GFP

BAG7 is a hallmark of UPR during heat stress and complexes with bZIP28 in the ER (Li et al., 2017; Nawkar et al., 2018). In response to heat stress, the transmembrane domain of BAG7 is removed by cleavage and BAG7 migrates to the nucleus. The truncated BAG7 associates with WRKY29 to upregulate genes involved in heat stress resistance. Because bZIP28 plays a role in restricting TuMV-GFP infection but has no role in PIAMV-GFP infection, we hypothesized that BAG7 is a factor restricting TuMV-GFP and not PIAMV-GFP.

We inoculated WT Col-0 and bag7 plants with TuMV-GFP, and monitored GFP fluorescence as before. At 8 dpi the average FVs were similar in WT and bag7 plants. Immunoblot analysis also showed that the CP levels were similar in *bag7* and WT Col-0 plants (Figure 3a–c; P < 0.05). We also recorded and statistically analyzed FVs in systemic leaves between 10 and 19 dpi (Figure 3b; n = 12). In these experiments, there was no difference in FVs in the upper leaves of Col-0 and bag7 plants (Figure 3b,c; P < 0.05). These results indicate that BAG7 does not restrict local or systemic TuMV-GFP infection.

We then inoculated Col-0 and bag7 plants with PIAMV-GFP, and we viewed these primary leaves at 5 dpi. We were surprised that the average FV was 6.9-fold higher in the bag7 than in the WT Col-0 inoculated leaves (Figure 3d; P < 0.05; n = 6). Immunoblots also showed the CP levels were markedly higher in bag7 compared with WT Col-0 leaves (Figure 3d). When we analyzed the FVs in systemic leaves between 10 and 19 dpi, there was no difference in FVs in the upper leaves of Col-0 and bag7 plants (Figure 3e,f; P < 0.05). These results demonstrate that BAG7 is important for restricting PIAMV-GFP local infection in the inoculated leaves, but does not restrict systemic infection.

TGB3 and 6K2 induce NAC089 and NAC103 expression

The NAC089 and NAC103 transcription factors are among the canonical UPR genes that are upregulated by bZIP60 and bZIP28. NAC089 regulates downstream genes involved in programmed cell death such as BAG6, while NAC103 activates downstream UPR genes including Calreticulin 1 and Calnexin1 and Protein disulfide isomerase 5 (Sun et al., 2013; Yang et al., 2014). We carried out experiments to learn whether these downstream UPR genes are upregulated in response to these viral elicitors. Binary plasmids expressing each TGB3 and 6K2 gene were delivered to WT Col-0, bzip60, bzip28, bzip17, bzip60/17 and bzip60/28 plants. We carried out RT-qPCR to quantify NAC089 and NAC103 transcript levels at 2 dpi. The average FVs after

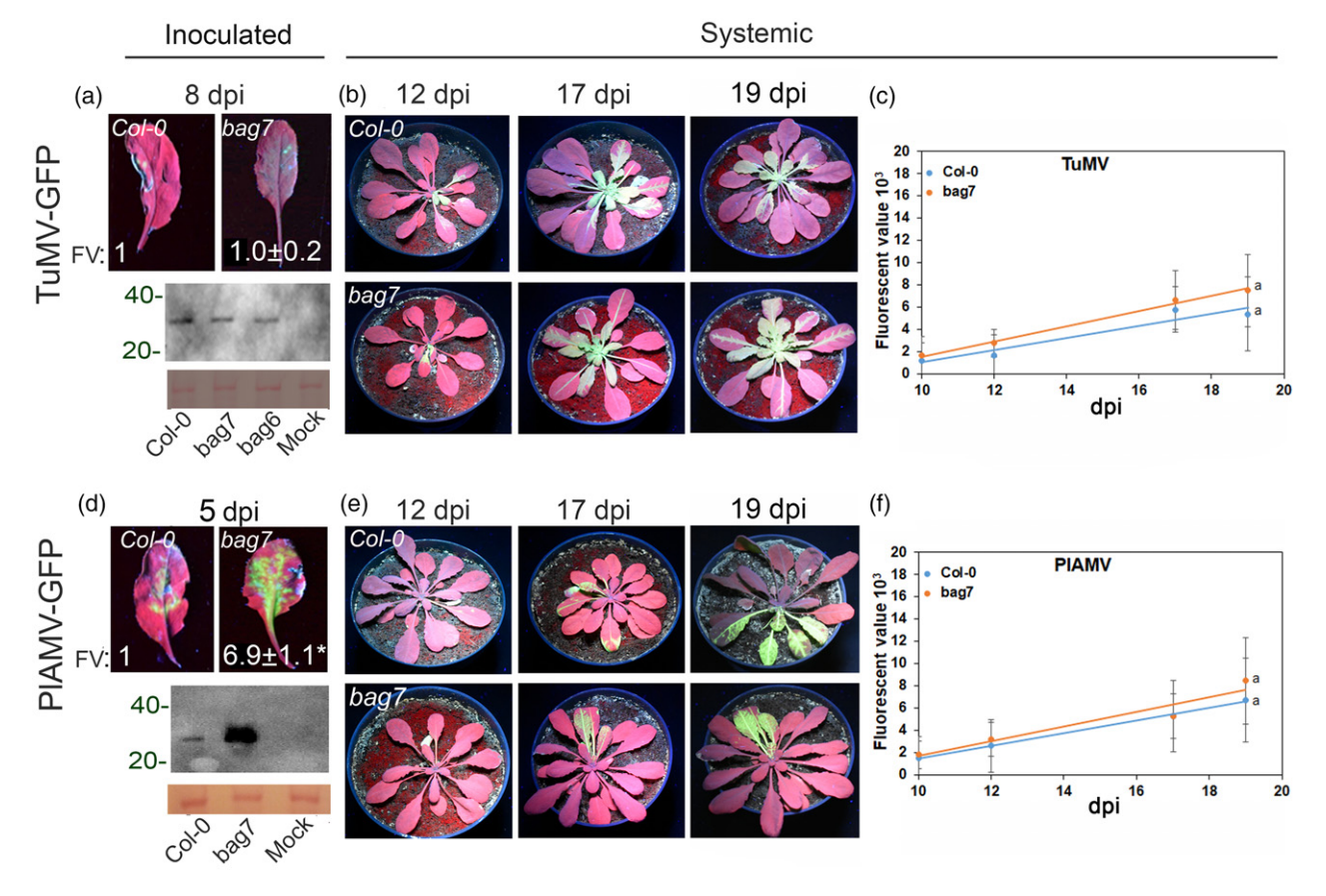


Figure 3. Local and systemic infection of PIAMV-GFP and TuMV-GFP in bag7 and Col-0 plants.

(a,d) Representative images of TuMV-GFP and PIAMV-GFP inoculated leaves at 5 and 8 days post-inoculation (dpi), respectively. The average fluorescence values (FVs), the SDs and statistical relatedness are reported at the bottom of each panel. Asterisks indicate statistical differences: Student's t-test; P < 0.05; n = 6. Immunoblot analysis detecting TuMV and PIAMV CPs in the inoculated leaves, respectively. Ponceau S-stained membrane below the immunoblot shows total equal protein loading.

(b,e) Representative images of plants infected with TuMV-GFP and PIAMV-GFP at 12, 17 and 19 dpi.

(c,f) Scatter plot values and trend lines represent the average FV and SDs for each mutant and Col-0 line inoculated with TuMV-GFP and PIAMV-GFP, respectively. Letters next to each trend line represent the statistical relatedness of the FVs for each treatment: Student's paired t-test; P < 0.05; n = 12.

delivery of each TGB3 or 6K2 were statistically compared with the FVs of the mock-treated samples.

In WT Col-0 plants, *NAC089* was induced between eightand 37-fold relative to the mock-treated control in leaves expressing the TGB3 or 6K2 proteins (Figure 4a; P < 0.05; n = 3). In *bzip60*, *bzip28* and *bzip17* plants, the levels of *NAC089* transcripts were obviously reduced compared with the WT Col-0 plants, although the transcript levels remained 2.3- to 5.6-fold above the mock-treated plants (Figure 4a; P < 0.05, n = 3). In *bzip60/bzip17* and *bzip60/bzip28* plants, there was no induction following treatment with each of these viral elicitors, suggesting an additive effect of the combined genes.

In Col-0 plants, NAC103 was induced by approximately 2.5- to fourfold following expression of the TGB3 or 6K2 proteins (Figure 4b; P < 0.05). In bzip17 and bzip28 plants, NAC103 expression ranged from three- to eightfold above the control leaves, except in the case of PVY 6K2, which

did not show a significant change in bzip28 plants. Gene induction was not observed in bzip60, bzip60/bzip17 and bzip60/bzip28 plants (Figure 4b; P < 0.05). These combined data suggest that TGB3 and 6K2 induced NAC089 and NAC103 expression in a manner that is dependent upon bZIP60.

NAC089, but not BAG6, reduces the systemic accumulation of PIAMV-GFP

NAC089 is a molecular relay from bZIP60, bZIP28 and bZIP17 to upregulate ER stress-responsive genes including BAG6 (Yang et~al., 2014). As in previous experiments, GFP was used as a reporter of PIAMV-GFP and TuMV-GFP systemic infection in nac089 and bag6 plants (Figure 5a; n=6). We could not test the role of NAC103 in virus infection because there are no available homozygous mutant lines (https://abrc.osu.edu) with altered NAC103 expression.

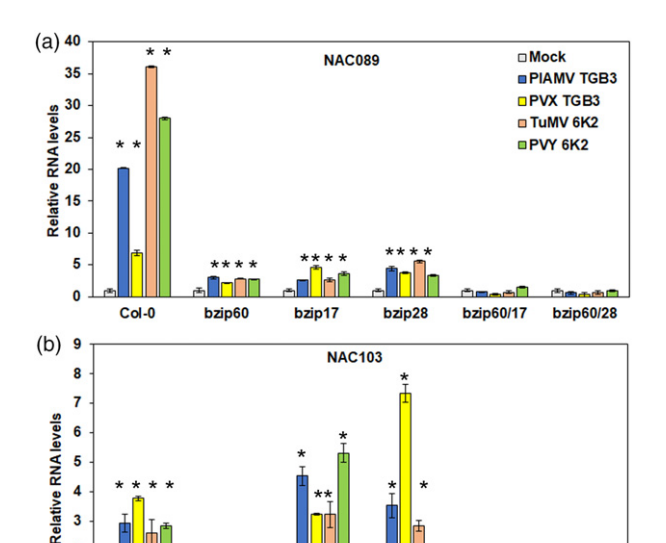


Figure 4. Overexpression of NAC089 and NAC103 in wild-type (WT) and bZIP mutants Arabidopsis leaves following agro-delivery of TGB3 and 6K2

bzip17

bzip28

bzip60/17

2

Col-0

Bar graphs depict the average relative NAC089 (a) and NAC103 (b) transcript levels in samples harvested at 2 days post-inoculation (dpi). Agro-delivery of each viral factor is identified in the chart legend in (a). Error bars represent SD, and asterisks indicate significant differences between treatments with viral factors and the mock: Student's t-test; P < 0.05; n = 3.

Among PIAMV-GFP inoculated plants, the FVs were significantly higher in nac089 than in Col-0 plants (Figure 5b; P < 0.05). However, the average FVs in Col-0 and bag6 plants were not significantly different (Figure 5b; P > 0.05). Regarding TuMV-GFP infection, the FVs in systemic leaves were unaltered in nac089 and bag6 compared with WT Col-0 plants (Figure 5d; P > 0.05).

BAG6 is a eukaryotic co-chaperone involved in protein quality control and proteasome elimination of malformed proteins (Kawahara et al., 2013; Yamamoto et al., 2017). The human BAG6 aids the folding of aggregation-prone proteins, polyubiquitinated proteins and transmembrane proteins. The AtBAG6 is associated with autophagy and disease resistance to B. cinerea (Li and Dickman, 2016). ATG8 lipidation is a hallmark of autophagic activity. We analyzed the lipidation pattern of ATG8 in ire1a/ire1b, bzip60, bzip28, bzip17, nac089 and bag6 plants. The accumulation of ATG8-PE was consistent across virus-inoculated WT and mutant Col-0 lines. These data suggest that autophagic activity during virus infection is not directly managed by these UPR pathways (Figure S2). Finally, these results suggest that NAC089 has a role in restricting PIAMV-GFP systemic accumulation, and that BAG6 is not involved in the systemic accumulation of either virus.

Increased protein folding capacity reduced PIAMV-GFP accumulation

Cells gain tolerance to ER stress by increasing the protein folding capacity of the ER through enhanced expression of chaperones. BiPs are among the major targets of UPR signaling pathways converging on their activation in response to ER stress. Because Arabidopsis *BiP1* and *BiP2* share 97% nucleotide and 99% amino acid sequence identities, their expression cannot be easily differentiated by RT-gPCR. BiP3 is 80% identical to BiP1/2, and PCR primers can differentially detect these transcripts (Noh et al., 2003; Srivastava et al., 2013). At 5 dpi, BiP1/2 transcripts were elevated following agro-delivery of TuMV or PVY 6K2 (Figure 6a; P < 0.05), but not following expression of PIAMV or PVX TGB3. However, BiP3 transcripts were elevated three- to fourfold above the control in response to expression of PIAMV TGB3, PVX TGB3, PVY 6K2 and TuMV 6K2 (Figure 6a: P < 0.05).

To examine the importance of the protein folding capacity in virus accumulation, we quantified virus-GFP fluorescence in infected plantlets grown on MS medium with added dithiothreitol (DTT) and tauroursodeoxycholic acid (TUDCA). DTT causes significant ER stress in plant cells by reducing protein disulfide bond formation and reducing the protein folding capacity. TUDCA is a chemical chaperone that alleviates ER stress when applied to plants because it mitigates protein aggregation and stabilizes protein conformation (Zhang et al., 2015; Fernández-Bautista et al., 2017; Uppala et al., 2017). We were unable to infect young plantlets with TuMV-GFP, and conducted these experiments only with PIAMV-GFP. Ten-day-old Col-0 plantlets were inoculated with PIAMV-GFP and transferred to MS medium alone, with added 0.1 mm DTT, or with added 0.5 mm TUDCA (Figure 6b,c). At 15 dpi, the plantlets were ground, and the fluorescence was measured in plant extracts using a fluorometer. The average FV relative to the average sample fresh weight was reported for each treatment (Figure 6c). The fluorescence levels in extracts of PIAMV-GFP-infected plantlets grown on DTT-containing medium were higher in extracts of infected plantlets grown on MS medium alone (Figure 6c; P < 0.05). These data suggest that compromising the protein folding capacity of the cell could favor virus infection. On the other hand, PIAMV-infected plantlets grown on the TUDCA-containing medium showed lower fluorescence than the controls (Figure 6c; P < 0.05), suggesting that the increased protein folding capacity leads to a decrease in virus accumulation.

We also grew bzip17, bzip28 and bzip60 plantlets infected with PIAMV-GFP on MS media alone, with 0.1 mm DTT, or with 0.5 mm TUDCA. These infected plantlets showed very slow growth on DTT-containing medium and could not be used to produce an adequate fluorescence dataset. Thus, we only analyzed infected plantlets grown on MS and TUDCA-containing medium. PIAMV-GFP

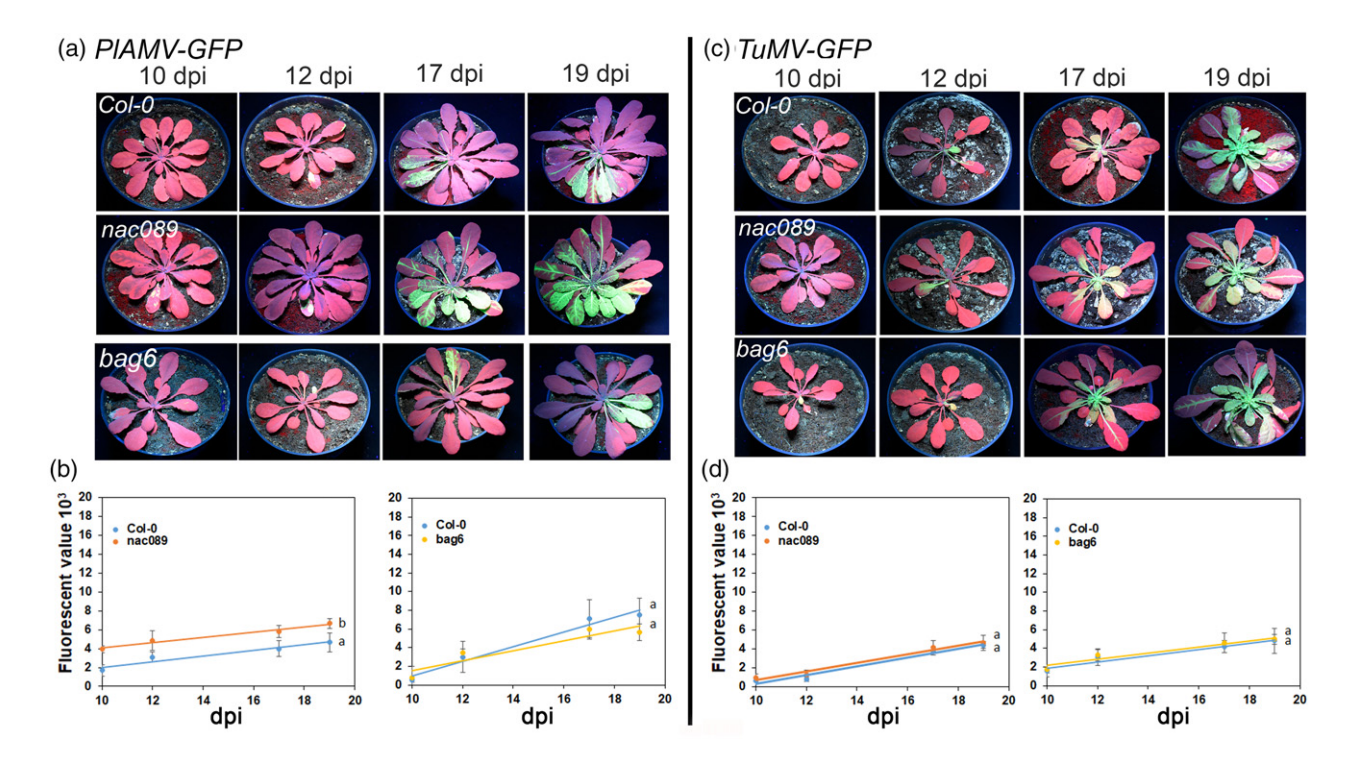


Figure 5. Local and systemic infection of PIAMV-GFP and TuMV-GFP in nac089 and bag6, and Col-0 plants.

(a,c) Representative images of Col-0, nac089 and bag6 plants infected with PIAMV-GFP or TuMV-GFP.

(b,d) Scatter plot values and trend lines represent the average fluorescence values (FVs) and SDs for each mutant line and Col-0 inoculated with PIAMV-GFP and TuMV-GFP. Letters next to each trend line represent the statistical relatedness of the FVs for each treatment: Student's paired t-test; P < 0.05; n = 6.

fluorescence was lower in bzip17, bzip28 and bzip60 plants grown on TUDCA medium compared with the fluorescence obtained from plants grown in regular MS media (Figure 6d; P < 0.05). These combined data demonstrate that TUDCA can mitigate mutations impacting UPR signaling during PIAMV-GFP infection. Finally, this result shows that expanding the protein folding capacity leads to decreased PIAMV-GFP accumulation, and suggests that the maintenance of the functional protein folding machinery is key for plants to restrict virus infection.

DISCUSSION

This study presents evidence that the bZIP17/bZIP28 pathway, alongside the IRE1/bZIP60 pathways, modulates the levels of PIAMV and TuMV infection in Arabidopsis plants. Regarding PIAMV-GFP, we showed higher virus accumulation in bzip17 and bzip60 than in WT and bzip28 plants, clearly demonstrating that both bZIP17 and bZIP60 have roles in restricting PIAMV local and systemic infection. These data also demonstrated that there was no significant difference between the average GFP FVs in bzip17 and bzip60 mutants, and that both factors serve to restrict PIAMV-GFP systemic accumulation. By comparing virus accumulation in bzip60 and bzip17 single KO with bzip60/bzip17 double KO plants, we noted higher PIAMV-GFP accumulation in the double KO plants, indicating that

bZIP17 and bZIP60 are additive and synergistic. Because bZIP60 and bZIP17 can created heterodimers for induce target genes (Vinson et al., 2006; Henriquez-Valencia et al., 2015), it is reasonable to suggest that bZIP60 and bZIP17 act as heterodimers for induce gene(s) that function to limit PIAMV-GFP accumulation. Given the hypothesis that bZIP60 restricts PIAMV-GFP accumulation, we expected that virus FVs in the bzip60/bzip28 plants would resemble the higher accumulation observed in bzip60 plants. However, the data presented here indicate that PIAMV-GFP accumulation is largely unaltered in bzip28 and bzip28/ bzip60 KO plants compared with WT Col-0 plants. Taking into consideration prior reports that bZIP28 and bZIP60 form homo- and hetero-dimers, these data presented in this study support a model in which bZIP28 and bZIP60 redundantly upregulate certain unknown factor(s) that support PIAMV accumulation.

Figure 7(a) presents a model in which bZIP60 and bZIP17 synergistically induce genes restricting PIAMV infection, while bZIP60 and bZIP28 independently induce genes supporting PIAMV infection. In bzip60 and bzip17 plants, genes restricting virus are not induced by bZIP17 or bZIP60 alone, whereas genes supporting PIAMV infection are induced by bZIP28, resulting in high virus accumulation. In bzip28 plants, genes restricting virus accumulation are induced by bZIP60 and bZIP17, and genes supporting

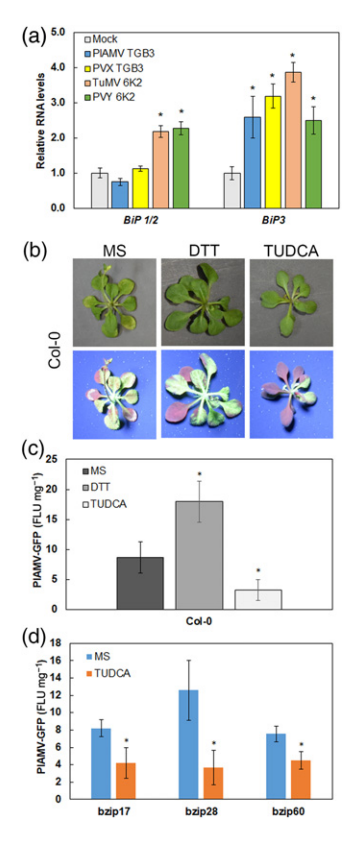


Figure 6. TUDCA represses PIAMV-GFP accumulation.

(a) Reverse transcriptase-quantitative polymerase chain reaction (RT-qPCR) results providing relative RNA levels of BiP1/2 and BiP3 following treatments with each viral factor identified by color in the chart legend. Error bars represent SD and asterisks indicate significant differences to the mock control: Student's t-test; P < 0.05; n = 3.

(b) Brightfield and fluorescent images of Col-0 plantlets grown on MS medium, 0.1 mm of dithiothreitol (DTT) or 0.5 mm of TUDCA containing medium and infected with PIAMV-GFP at 15 days post-inoculation (dpi).

(c) Fluorescence from PIAMV-GFP-infected Col-0 plantlets grown on MS medium, 0.1 mm of DTT or 0.5 mm of TUDCA-containing medium at 15 dpi. Results are expressed in arbitrary fluorescence units per fresh weight (FLU mg⁻¹). The error bars represent SD and asterisks indicate significant difference from plantlet on MS medium: Student's t-test: P < 0.05: n = 3-4.

(d) Fluorescence from PIAMV-GFP-infected bzip17, bzip28 and bzip60 mutant plantlets grown on MS medium or 0.5 mm of TUDCA-containing medium at 15 dpi (FLU mg⁻¹). The error bars represent SD, and asterisks indicate significant difference between treatment and non-treated samples: Student's *t*-test; P < 0.05; n = 3-4.

PIAMV infection are induced by bZIP60 resulting in moderate virus accumulation, as in WT Col-0 plants. Finally, in bzip60/bzip28 plants, the phenotype observed in bzip60 plants is alleviated by the absence of supporting genes induction by bZIP28.

Regarding TuMV-GFP infection, Figure 7(b) presents a model in which bZIP60 and bZIP28 serve to repress local and systemic infection. TuMV-GFP accumulation was not altered in bzip17 plants compared with WT Col-0 plants, suggesting that bZIP17 is not a factor in restricting TuMV infection. The results in Figure 2 show that GFP FVs measured in systemic leaves were comparable between bzip60,

bzip28 and bzip60/bzip28 plants. These data indicate that bZIP28 and bZIP60 restrict TuMV-GFP, but are not additive in their effects on TuMV-GFP accumulation. These results show that bZIP60 and bZIP28 synergistically activate genes that restrict potyvirus accumulation. In contrast to PIAMV-GFP infection, TuMV-GFP infection does not seem to be supported by any UPR signaling pathway. Consequently, KO-mutations of bZIP60, bZIP28 or both lead to higher virus infection, whereas a KO mutation of bZIP17 has no effect (Figure 7b).

It is well accepted that bZIP transcription factors form heterodimers with other bZIP factors to expand the diversity of ER stress-induced genes that they can activate. Many reports showed that bZIP17, bZIP28 and bZIP60 coregulate certain genes in a manner that can expand the pattern of tissue expression, the timing of gene induction, or the magnitude of the response (Liu and Howell, 2010; Henriquez-Valencia et al., 2015; Angelos et al., 2017; Kim et al., 2018; Ruberti et al., 2018). On the other hand, these bZIP transcription factors can also act alone, as homodimers, to activate certain downstream genes. For example, bZIP60 directly binds the cis-element pUPRE-III, whereas only bZIP17 can activate some specific downstream transcription responses in response to salt stress. Our results support these mechanisms as bZIP60 can act independently of bZIP28 for support with PIAMV infection or in synergy with bZIP17 or bZIP28 to repress PIAMV and TuMV infection, respectively. Consequently, the different abilities of bZIP17, bZIP28 and bZIP60 to bind cis-regulatory elements of UPR genes explain the different observations between PIAMV and TuMV infection.

There is a significant body of research using ER stressinducing agents such as tunicamycin or DTT to investigate the molecular basis of adaptive UPR. ER stress recovery, or cell fate. These studies typically examine root and shoot growth of seedlings following short-term or chronic treatments with ER stress-inducing agents. The most recent working model suggests that bZIP28 and bZIP60 act in parallel to modulate common ER stress-responsive genes engaged in adaptive UPR and ER stress recovery as well as chronic ER stress (Angelos et al., 2017; Ruberti et al., 2018). The bZIP17 and bZIP28 jointly support the expression of genes involved in root elongation and vegetative growth. By employing PIAMV and TuMV to infect Arabidopsis plants, we were able to contrast the requirements for bZIP factors in UPR activation in aerial parts of Arabidopsis plants and determined that bZIP17, along with bZIP28 and bZIP60, specifically recognizes PIAMV TGB3 to activate genes that support ER homeostasis during virus infection.

BAG7 is an ER sensor of UPR and a co-factor for WRKY29 transcriptional activation in the nucleus. Because bZIP28 activation is linked to complex dissociation of bZIP28/BAG7/BiPs (Li et al., 2017), we expected that TuMV-GFP accumulation in the bag7 plants should be restricted.

We were surprised that the data show that PIAMV-GFP and not TuMV-GFP is affected by BAG7. Evidence that PIAMV-GFP local infection in bag7 inoculated leaves is higher than in WT Col-0 inoculated leaves suggests that BAG7 is an early response gene to potexvirus infection. Further experiments are needed to test whether virus suppression is the result of BAG7 chaperone functions in the ER and/or BAG7-WRKY29 interactions in the nucleus. The hypothesis that BAG7-WRKY29 gene regulation is a factor in virus infection is particularly intriguing because WRKY29 is engaged in pattern-triggered immunity. Overexpressing WRKY29 may enhance disease resistance to Fusarium graminearum infection and other pathogens (Asai et al., 2002; Sarowar et al., 2019). It is reasonable to consider that the PIAMV TGB3 protein might activate UPR in a manner that produces cytoprotective chaperones while also managing anti-viral immunity.

Downstream of bZIP60, bZIP28 and bZIP17, UPR signaling is relayed by key NAC transcription factors (Nawkar

et al., 2018). This study demonstrates that NAC089 and NAC103 are overexpressed after TGB3 and 6K2 transient expression. TuMV-GFP accumulation was similar in nac089 and Col-0 plants, revealing that NAC089 is not a factor in restricting TuMV infection. On the other hand, PIAMV-GFP accumulation was slightly but significantly higher in nac089 than in Col-0 plants, suggesting that NAC089 is a factor in restricting PIAMV infection.

The UPR activity is mainly associated with the increase of the protein folding capacity of the ER through enhanced expression of the chaperones such as *BiP*, *CRT*, *CNX* and *PDI*. We previously demonstrated that TGB3 activates expression of *CRT2* and *PDI* in Arabidopsis and *N. benthamiana* (Ye *et al.*, 2011), and this study demonstrated that TGB3 and 6K2 induce expression of *BiPs*. Overexpression of *N. tabacum BiP-like protein 4* protects against viral-induced necrosis (Leborgne-Castel *et al.*, 1999; Ye and Verchot, 2011; Ye *et al.*, 2011). Here we show that the cellular protein folding capacity strongly influences Arabidopsis

(a) UPR regulation of PIAMV infection

Col-0 bzip60 bZIP17 bZIP60 bZIP28 bZIP17 b**2**60 bZIP28 Virus Virus Virus Virus restriction infection restriction infection → Regular PIAMV infection → High PIAMV accumulation bzip28 bzip60/bzip28 bZIP17 bZIP60 b**2** 28 bZIP17 b**2 K**60 Virus Virus Virus Virus restriction infection restriction infection → Regular PIAMV infection → Regular PIAMV infection bzip17 bzip60/bzip17 b**XX**17 bZIP60 bZIP28 bZIP28 Virus Virus Virus Virus restriction infection restriction infection → High PIAMV accumulation → High PIAMV accumulation

(b) UPR regulation of TuMV infection

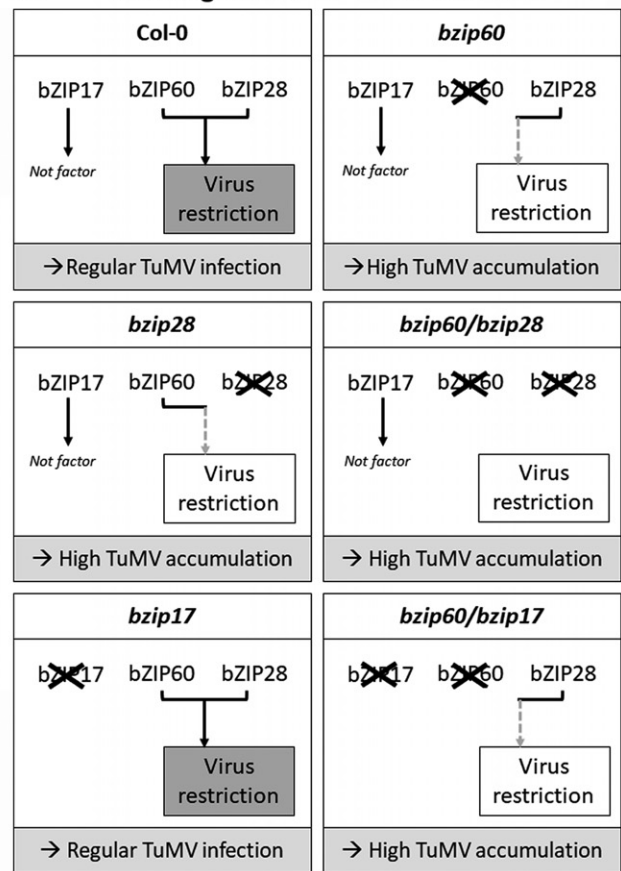


Figure 7. Proposed model for the function of UPR during PIAMV and TuMV infection.

(a) During PIAMV infection, bZIP28 and bZIP60 redundantly upregulate certain unknown factor(s) providing positive support for PIAMV infection (dark box) and bZIP17 and bZIP60 synergistically upregulate factor restricting PIAMV infection (gray box).

(b) During TuMV infection, bZIP28 and bZIP60 synergistically upregulate factor restricting TuMV infection (gray box) whereas bZIP17 is not a factor involve in TuMV infection.

susceptibility to virus infection. Increasing the folding capacity of Arabidopsis through DTT and TUDCA application leads to a significant increase or decrease of the PIAMV-GFP accumulation. Altogether these results suggest that during virus infection, UPR serves to maintain a functional protein folding machinery for repress virus accumulation. The role of the protein folding machinery in virus inhibition is not clear, but one can imagine that virus strongly recruits the folding protein machinery for its own benefit, and consequently host proteins dedicated to biotic stress defense are not folded properly. Under these conditions, increasing the protein folding capacity could permit the cell to protect and promote its defense machinery. However, regarding the synergic action of bZIP factors involved in UPR-associated virus inhibition and differences observed between PIAMV and TuMV, the role of UPR is probably not limited to protein folding capacity and further experiments are needed to clearly define the interactions that repress virus accumulation.

In conclusion, this study provides evidence of the role of bZIP17 under chronic ER stress led by virus infection. We reveal that the two UPR arms seem to be mainly associated with virus inhibition, at the exception of downstream factors of bZIP28 during PIAMV infection, and probably repress virus accumulation by increasing protein folding capacity. The diversity of these mechanisms reveals a finetuning of UPR in plants following virus infection.

EXPERIMENTAL PROCEDURES

Plant materials

Arabidopsis thaliana ecotype Columbia-0 (Col-0) and KO independent homozygous transfer DNA (T-DNA) insertion lines; bZIP60-2 (SAIL_283_B03), bZIP17 (SALK_104326), bZIP28-2 (SALK_132285), nac089 (SALK_201394), bag6-1 (SALK_047959), bag7 (Salk_065883), bZIP60-2/28-2, bZIP60-2/17 and IRE1a-2/1b-4 were obtained from ABRC (Ohio State University, Columbus, OH, USA), verified by PCR and maintained in the laboratory (Williams et al., 2010; Gaguancela et al., 2016; Li et al., 2016). All Arabidopsis plants were grown in a growth room with long-day (16 h) or short-day (12 h) photoperiod at 23°C.

Virus infection assay and transient expression of viral factors

The pMDC32 and pGWB505 binary vectors containing PVY 6K2, TuMV 6K2, PVX TGB3 or PIAMV TGB3 genes were used for transient delivery to Arabidopsis leaves, and previously reported (Gaguancela et al., 2016; ThermoFisher, Richardson, TX, USA). The pGWB505 constructs had GFP fused to the 3'-end of the viral genes. Agrobacterium harboring empty pMDC32 or GFP expression vector pXF7FNF2.0 were used as Mock. GFP-tagged infectious clones of TuMV and PIAMV were reported previously (Gaguancela et al., 2016). All plasmids were verified by sequencing and maintained in A. tumefaciens (GV3101). Liquid cultures harboring the relevant expression constructs were suspended in a solution of 10 mm MES-KOH (pH 5.6), 10 mm MgCl₂, 200 μm acetosyringone and adjusted to OD600 = 0.7-1.0. A 1-ml needle-free syringe was used to infiltrate the agrobacterium suspensions into leaves of 3-week-old Arabidopsis seedlings grown under shortday conditions. The timeline of PIAMV-GFP and TuMV-GFP infection is detailed in Figure S1.

RNA extraction and real-time RT-PCR

Leaf punches were harvested and immediately ground into powder in liquid nitrogen using 1600 MiniG Automated Tissue Homogenizer and Cell Lyser (SPEX Sample Prep, Metuchen, NJ, USA). RNA extraction was carried out using the Maxwell LEV simplyRNA purification kit (Promega, Madison WI, USA) or RNeasy Mini kit (Qiagen, Valencia, CA, USA). One microgram of RNA, the high-capacity cDNA reverse transcription kit (ThermoFisher, Richardson, TX, USA) and random primers were employed for cDNA synthesis. All PCR primers are provided in Table S1. For the qPCR assays, the efficiencies of all primers were verified by endpoint PCR and gel electrophoresis. Transcript abundance was quantified using Power SYBR Green II PCR master mix (ThermoFisher) in the ABI 7500 PCR and Step-One Plus or the QuantSudio 3 machines (Applied Biosystems, Foster City, CA, USA). The relative increase of cellular transcripts was calculated using the comparative cycle threshold (CT) method, which employs the equation 2^{-ddCT}. The endogenous control was ubiquitin-10 or 18S. Statistical analysis was carried out using Student's t-test to validate the results.

Endpoint PCR detection of bZIP60u and bZIP60s assay was conducted using the primers described in Gaguancela et al. (2016). PCR amplification was carried out using GoTaq Green Master mix (Promega, Madison, WI, USA) and a C1000 thermal cycler (Bio-Rad, Hercules, CA, USA) using the following PCR conditions. Following denaturation at 95°C for 2 min, 40 cycles of denaturation at 95°C for 30 sec, annealing at 62°C for 30 sec, and elongation at 72°C for 20 sec in a 50-µl reaction. PCR products were visualized using 2% agarose gel using ChemiDoc MP imaging system (Bio-Rad). The gel profile was analyzed using IMAGE LAB Software™ version 6.0.1 (Bio-Rad).

Immunoblot analysis

For detecting viral proteins, immunoblot analysis was carried out using virus-infected inoculated leaves, harvested at 5 or 8 dpi for PIAMV-GFP or TuMV-GFP, respectively. PIAMV-GFP fluorescence appears earlier than TuMV-GFP fluorescence in inoculated leaves. Total protein was extracted using standard methods (Ye et al., 2011) and quantified using the Pierce™ Coomassie Plus assay (Thermo Scientific). Nine micrograms of protein was loaded onto 15% sodium dodecyl sulfate-polyacrylamide gel electrophoresis (SDS-PAGE) gels. For ATG8 detection, systemic infected leaves were harvested 25 dpi, and protein was extracted using a buffer comprised of 50 mm NaH₂PO₄ (pH 7.0), 200 mm NaCl, 10 mm MgCl₂, 10% glycerol, 0.2% β-mercaptoethanol and protease inhibitor cocktail (Sigma, St Louis, MO, USA). Fifteen micrograms of protein was loaded onto 15% SDS-PAGE gels containing 6 м urea. In both experiments the gels were transblots using Trans-Blot® Turbo™ Transfer System (Bio-Rad), and blots were probed with antisera detecting viral CPs obtained from Agdia (Elkhardt, IN, USA) or Atg8 from Abcam (Cambridge, UK).

Analysis of local and systemic infection

Analysis of local and systemic infection was previously optimized and reported (Gaguancela et al., 2016). For the local infection analyses, fluorescent images were acquired at 5 and 8 dpi after inoculation of PIAMV-GFP or TuMV-GFP, respectively. For the systemic infection analyses, fluorescent images were acquired between 10 and 19 dpi. IMAGE J software was used to quantify the fluorescent

intensity. The results represent the average FV for at least six plants. For comparisons of inoculated leaves, the FVs for each treatment were reported relative to the control. For comparisons of systemic infection, the values were plotted, and ANOVA (P < 0.05) was used to validate the results.

Chaperone protection assays

Arabidopsis seeds were sterilized with bleach 50%, Triton X-100 1% for 10 min, and washed five times with sterile water. Seeds were stratified for 3 days at 4°C, then germinated on solid (0.8% agar) ½-strength Murashige and Skoog medium including 2% glucose (½-MS) in a growth chamber for 10 days in long-day conditions. Seedlings were then vacuum infiltrated with the infectious clones of PIAMV-GFP (OD600 = 0.5-0.7). After infiltration, seedlings were transferred to liquid 1/2-MS medium for 24 h, and washed with ½-MS medium containing 100 μg ml⁻¹ timentin. Seedlings were then cultivated on solid 1/2-MS medium containing 100 μg ml⁻¹ timentin, complemented with 01 mm DTT or 0.5mm TUDCA. Plantlets were harvested at 15 dpi and ground in liquid nitrogen before GFP extraction in PBS buffer. GFP fluorescence was quantified with a Fluoroskan FL microplate fluorometer (Ex/ Em = 485 nm/538 nm). The results were expressed in arbitrary fluorescence units per fresh weight (FLU mg⁻¹) and represented the average of three-four plants. The significant differences were assessed by t-test (P < 0.05).

ACKNOWLEDGEMENT

The authors thank Steven Howell for providing the homozygous mutant lines used in this study. This research was funded by NSF/USDA-AFRI joint award number 1759034.

AUTHOR CONTRIBUTIONS

MG, MD, VH and JV designed research; MG, OAG, EV and VH performed research; MG, AOG, VH, FJF and JV analyzed data; MG, OAG, VH, FJF and JV wrote the paper.

CONFLICT OF INTEREST STATEMENT

The authors declare no conflicts of interest.

DATA AVAILABILITY STATEMENT

All gene sequences were deposited in GenBank. Public release of data will occur through the OAK TRUST Digital Repository at Texas A&M University and in accordance with NSF policies. Materials may be transferred to others under the terms of a material transfer agreement.

SUPPORTING INFORMATION

Additional Supporting Information may be found in the online version of this article.

Figure S1. Timeline of PIAMV-GFP and TuMV-GFP infection in Col-

Figure S2. ATG8 lipidation following PIAMV-GFP and TuMV-GFP infection.

Table S1. Primers used in this study.

REFERENCES

Angelos, E., Ruberti, C., Kim, S.-J. and Brandizzi, F. (2017) Maintaining the factory: the roles of the unfolded protein response in cellular homeostasis in plants. *Plant J.* **90**, 671–682.

- Asai, T., Tena, G., Plotnikova, J., Willmann, M.R., Chiu, W.-L., Gomez-Gomez, L., Boller, T., Ausubel, F.M. and Sheen, J. (2002) MAP kinase signalling cascade in Arabidopsis innate immunity. *Nature*, 415, 977–983.
- Bao, Y., Bassham, D.C. and Howell, S.H. (2019) A functional unfolded protein response is required for normal vegetative development. *Plant Physiol.* 179(4), 1834–1843.
- Bao, Y. and Howell, S.H. (2017) The unfolded protein response supports plant development and defense as well as responses to abiotic stress. Front. Plant Sci. 8, 1–6.
- Bao, Y., Pu, Y., Yu, X., Gregory, B.D., Srivastava, R., Howell, S.H. and Bassham, D.C. (2018) IRE1B degrades RNAs encoding proteins that interfere with the induction of autophagy by ER stress in *Arabidopsis thaliana*. *Autophagy*, 14, 1562–1573.
- Cabanillas, D.G., Jiang, J., Movahed, N., Germain, H., Yamaji, Y., Zheng, H. and Laliberté, J.-F. (2018) Turnip mosaic virus uses the SNARE protein VTI11 in an unconventional route for replication vesicle trafficking. *Plant Cell*, 30, 2594–2615.
- Che, P., Bussell, J.D., Zhou, W., Estavillo, G.M., Pogson, B.J. and Smith, S.M. (2010) Signaling from the endoplasmic reticulum activates brassinosteroid signaling and promotes acclimation to stress in Arabidopsis. Sci. Signal. 3, 1–12.
- Deng, Y., Srivastava, R. and Howell, S.H. (2013) Protein kinase and ribonuclease domains of IRE1 confer stress tolerance, vegetative growth, and reproductive development in Arabidopsis. *Proc. Natl Acad. Sci. USA*, 110, 19 633–19 638.
- Deppmann, C.D. (2004) Dimerization specificity of all 67 b-ZIP motifs in Arabidopsis thaliana: a comparison to Homo sapiens b-ZIP motifs. Nucleic Acids Res. 32, 3435–3445.
- Ezer, D., Shepherd, S.J., Brestovitsky, A. et al. (2017) The G-Box transcriptional regulatory code in Arabidopsis. Plant Physiol. 175, 628–640.
- Ezer, D., Zabet, N.R. and Adryan, B. (2014) Homotypic clusters of transcription factor binding sites: a model system for understanding the physical mechanics of gene expression. *Comput. Struct. Biotechnol. J.* 10, 63–69.
- Fernández-Bautista, N., Fernández-Calvino, L., Muñoz, A. and Castellano, M.M. (2017) HOP3, a member of the HOP family in Arabidopsis, interacts with BiP and plays a major role in the ER stress response. *Plant Cell Environ.* 40(8), 1341–1355.
- Gaguancela, O., Zúñiga, L.P., Arias, A.V., Halterman, D., Flores, F.J., Johansen, I.E., Wang, A., Yamaji, Y. and Verchot, J. (2016) The IRE1/bZIP60 pathway and Bax inhibitor 1 suppress systemic accumulation of potyviruses and potexviruses in *Arabidopsis* and *Nicotiana benthamiana* plants. *Mol. Plant–Microbe Interact.* 29, 750–766.
- Grangeon, R., Jiang, J., Wan, J., Agbeci, M., Zheng, H. and Laliberté, J.-F. (2013) 6K2-induced vesicles can move cell to cell during turnip mosaic virus infection. Front. Microbiol. 4, 1–10.
- Henriquez-Valencia, C., Moreno, A.A., Sandoval-Ibañez, O., Mitina, I., Blanco-Herrera, F., Cifuentes-Esquivel, N. and Orellana, A. (2015) bZIP17 and bZIP60 regulate the expression of BiP3 and other salt stress responsive genes in an UPR-independent manner in Arabidopsis thaliana. J. Cell. Biochem. 116, 1638–1645.
- Iwata, Y., Ashida, M., Hasegawa, C., Tabara, K., Mishiba, K. and Koizumi, N. (2017) Activation of the Arabidopsis membrane-bound transcription factor bZIP28 is mediated by site-2 protease, but not site-1 protease. *Plant J.* 91, 408–415.
- Iwata, Y. and Koizumi, N. (2005) An Arabidopsis transcription factor, Atb-ZIP60, regulates the endoplasmic reticulum stress response in a manner unique to plants. Proc. Natl Acad. Sci. USA, 102, 5280–5285.
- Iwata, Y., Yoneda, M., Yanagawa, Y. and Koizumi, N. (2009) Characteristics of the nuclear form of the Arabidopsis transcription factor AtbZIP60 during the endoplasmic reticulum stress response. *Biosci. Biotechnol. Biochem.* 73, 865–869.
- Kawahara, H., Minami, R. and Yokota, N. (2013) BAG6/BAT3: Emerging roles in quality control for nascent polypeptides. *J. Biochem.* **153**, 147–160.
- Kim, J.-S., Yamaguchi-Shinozaki, K. and Shinozaki, K. (2018) ER-anchored transcription factors bZIP17 and bZIP28 regulate root elongation. *Plant Physiol.* 176, 2221–2230.
- Leborgne-Castel, N., Jelitto-Van Dooren, E.P., Crofts, A.J. and Denecke, J. (1999) Overexpression of BiP in tobacco alleviates endoplasmic reticulum stress. *Plant Cell*, 11, 459–470.
- Li, F.F., Sun, H.J., Jiao, Y.B., Wang, F.L., Yang, J.G. and Shen, L.L. (2018) Viral infection-induced endoplasmic reticulum stress and a membrane-

- associated transcription factor NbNAC089 are involved in resistance to virus in Nicotiana benthamiana. Plant Path. 67, 233-243.
- Li, Y. and Dickman, M. (2016) Processing of AtBAG6 triggers autophagy and fungal resistance. Plant Signal. Behav. 11, e1175699.
- Li, Y., Kabbage, M., Liu, W. and Dickman, M.B. (2016) Aspartyl protease-mediated cleavage of BAG6 is necessary for autophagy and fungal resistance in plants. Plant Cell, 28, 233-247.
- Li, Y., Williams, B. and Dickman, M. (2017) (BAG7) -mediated heat tolerance requires translocation, sumoylation and binding to WRKY29. New Phytol.
- Liu, J.X. and Howell, S.H. (2010) bZIP28 and NF-Y transcription factors are activated by ER stress and assemble into a transcriptional complex to regulate stress response genes in Arabidopsis. Plant Cell, 22, 782-796.
- Liu, Y., Burgos, J.S., Deng, Y., Srivastava, R., Howell, S.H. and Bassham, D.C. (2012) Degradation of the endoplasmic reticulum by autophagy during endoplasmic reticulum stress in Arabidopsis. Plant Cell, 24, 4635-4651.
- Nagashima, Y., Mishiba, K., Suzuki, E., Shimada, Y., Iwata, Y. and Koizumi, N. (2011) Arabidopsis IRE1 catalyses unconventional splicing of bZIP60 mRNA to produce the active transcription factor, Sci. Rep. 1, 29.
- Nawkar, G.M., Lee, E.S., Shelake, R.M., Park, J.H., Ryu, S.W., Kang, C.H. and Lee, S.Y. (2018) Activation of the transducers of unfolded protein response in plants. Front. Plant Sci. 9, 214.
- Noh, S.-J., Kwon, C.S., Oh, D.-H., Moon, J.S. and Chung, W.-I. (2003) Expression of an evolutionarily distinct novel BiP gene during the unfolded protein response in Arabidopsis thaliana. Gene, 311, 81–91.
- Park, S.-H., Li, F., Renaud, J., Shen, W., Li, Y., Guo, L., Cui, H., Sumarah, M. and Wang, A. (2017) NbEXPA1, an α-expansin, is plasmodesmata-specific and a novel host factor for potyviral infection. Plant J. 92, 846-861.
- Ruberti, C., Lai, Y.S. and Brandizzi, F. (2018) Recovery from temporary endoplasmic reticulum stress in plants relies on the tissue-specific and largely independent roles of bZIP28 and bZIP60, as well as an antagonizing function of BAX-Inhibitor 1 upon the pro-adaptive signaling mediated bv bZIP28. Plant J. 93, 155-165.
- Sarowar, S., Alam, S.T., Makandar, R., Lee, H., Trick, H.N., Dong, Y. and Shah, J. (2019) Targeting the pattern-triggered immunity pathway to enhance resistance to Fusarium graminearum. Mol. Plant Pathol. 20,
- Shen, L., Li, F., Dong, W., Liu, W., Qian, Y., Yang, J., Wang, F. and Wu, Y. (2017) Nicotiana benthamiana NbbZIP28, a possible regulator of unfolded protein response, plays a negative role in viral infection. Eur. J. Plant Pathol. 149, 831-843.
- Srivastava, R., Deng, Y., Shah, S., Rao, A.G. and Howell, S.H. (2013) BIND-ING PROTEIN is a master regulator of the Endoplasmic reticulum stress sensor/transducer bZIP28 in Arabidopsis. Plant Cell, 25, 1416-1429.
- Srivastava, R., Li, Z., Russo, G. et al. (2018) Response to persistent ER stress in plants: a multiphasic process that transitions cells from prosurvival activities to cell death. Plant Cell, 30, 1220-1242.

- Sun, L., Lu, S.J., Zhang, S.S., Zhou, S.F., Sun, L. and Liu, J.X. (2013a) The lumen-facing domain is important for the biological function and organelle-to-organelle movement of BZIP28 during ER stress in arabidopsis. Mol. Plant. 6, 1605-1615.
- Sun, L., Yang, Z.-T., Song, Z.-T., Wang, M.-J., Sun, L.e., Lu, S.-J. and Liu, J.-X. (2013b) The plant-specific transcription factor gene NAC103 is induced by bZIP60 through a new cis -regulatory element to modulate the unfolded protein response in Arabidopsis. Plant J. 76, 274-286.
- Tilsner, J., Linnik, O., Louveaux, M., Roberts, I.M., Chapman, S.N. and Oparka, K.J. (2013) Replication and trafficking of a plant virus are coupled at the entrances of plasmodesmata. J. Cell Biol. 201, 981-
- Uppala, J.K., Gani, A.R. and Ramaiah, K.V.A. (2017) Chemical chaperone, TUDCA unlike PBA, mitigates protein aggregation efficiently and resists ER and non-ER stress induced HepG2 cell death. Sci. Rep. 7, 3831.
- Verchot-Lubicz, J., Torrance, L., Solovyev, A.G., Morozov, S.Y., Jackson, A.O. and Gilmer, D. (2010) Varied movement strategies employed by triple gene block-encoding viruses. Mol. Plant-Microbe Interact. 23, 1231-1247.
- Verchot, J. (2016) Plant virus infection and the ubiquitin proteasome machinery: arms race along the endoplasmic reticulum. Viruses. 8, 314.
- Vinson, C., Acharya, A. and Taparowsky, E.J. (2006) Deciphering b-ZIP transcription factor interactions in vitro and in vivo. Biochim. Biophys. Acta -Gene Struct. Exp. 1759, 4-12.
- Williams, B., Kabbage, M., Britt, R. and Dickman, M.B. (2010) AtBAG7, an Arabidopsis Bcl-2-associated athanogene, resides in the endoplasmic reticulum and is involved in the unfolded protein response. Proc. Natl. Acad. Sci. USA, 107, 6088-6093.
- Yamamoto, K., Hayashishita, M., Minami, S., Suzuki, K., Hagiwara, T., Noguchi, A. and Kawahara, H. (2017) Elimination of a signal sequenceuncleaved form of defective HLA protein through BAG6. Sci. Rep. 7, 14
- Yang, J. and Zhang, Y. (2015) I-TASSER server: new development for protein structure and function predictions. Nucleic Acids Res. 43, W174-W181.
- Yang, Z.T., Wang, M.J., Sun, L.L. et al. (2014) The membrane-associated transcription factor NAC089 controls ER-stress-induced programmed cell death in plants. PLoS Genet. 10, e1004243.
- Ye, C., Dickman, M.B., Whitham, S.A., Payton, M. and Verchot, J. (2011) The unfolded protein response is triggered by a plant viral movement protein. Plant Physiol. 156, 741-755.
- Ye, C. and Verchot, J. (2011) Role of unfolded protein response in plant virus infection. Plant Signal. Behav. 6, 1212-1215.
- Zhang, L., Chen, H., Brandizzi, F., Verchot, J. and Wang, A. (2015) The UPR branch IRE1-bZIP60 in plants plays an essential tole in viral infection and is complementary to the only UPR pathway in yeast. PLOS Genet. 11, e1005164